applied sciences

MDPI

Review

3D and 4D Printing of Multistable Structures

Hoon Yeub Jeong [1,*], Soo-Chan An [1], Yeonsoo Lim [1], Min Ji Jeong [1], Namhun Kim [2] and Young Chul Jun [1,*]

[1] School of Materials Science and Engineering, Ulsan National Institute of Science and Technology (UNIST), Ulsan 44919, Korea; soo7913@unist.ac.kr (S.-C.A.); dustn7792@unist.ac.kr (Y.L.); jmj703s@naver.com (M.J.J.)

[2] School of Mechanical, Aerospace and Nuclear Engineering, UNIST, Ulsan 44919, Korea; nhkim@unist.ac.kr

* Correspondence: hyjeong@unist.ac.kr (H.Y.J.); ycjun@unist.ac.kr (Y.C.J.)

Received: 30 September 2020; Accepted: 14 October 2020; Published: 16 October 2020

Abstract: Three-dimensional (3D) printing is a new paradigm in customized manufacturing and allows the fabrication of complex structures that are difficult to realize with other conventional methods. Four-dimensional (4D) printing adds active, responsive functions to 3D-printed components, which can respond to various environmental stimuli. This review introduces recent ideas in 3D and 4D printing of mechanical multistable structures. Three-dimensional printing of multistable structures can enable highly reconfigurable components, which can bring many new breakthroughs to 3D printing. By adopting smart materials in multistable structures, more advanced functionalities and enhanced controllability can also be obtained in 4D printing. This could be useful for various smart and programmable actuators. In this review, we first introduce three representative approaches for 3D printing of multistable structures: strained layers, compliant mechanisms, and mechanical metamaterials. Then, we discuss 4D printing of multistable structures that can help overcome the limitation of conventional 4D printing research. Lastly, we conclude with future prospects.

Keywords: 3D printing; 4D printing; multistability; compliant mechanism; mechanical metamaterial; smart actuator

1. Introduction

Three-dimensional (3D) printing, also called additive manufacturing, is a new paradigm in customized manufacturing. Compared to traditional subtractive manufacturing methods, 3D printing allows a bottom-up fabrication of complex 3D objects that are hard to create with conventional fabrication methods [1]. By using appropriate 3D printing techniques, various materials, such as metal powders, polymers, ceramics, and composites, can be printed in high resolution. It also reduces material waste during production. Therefore, 3D printing provides a cost-effective solution for prototyping, optimization, and customization. Because of these advantages, an increasing number of industries and sectors are adopting 3D printing [2–5].

Figure 2 schematically explains various 3D printing processes. Stereolithography (SLA) uses photopolymerization to solidify photocurable liquids and create 3D structures. Photopolymers are cured by laser light, and the exposed portion of the polymers hardens. After each laser pass, the build plate moves down slightly until the 3D structure is completed. This idea was first introduced in 1984 [6] and, since then, many other 3D printing techniques have been invented. Digital light processing (DLP) is similar to SLA, but it can expose an entire layer at once using a projector, thus enabling large printing volumes at high speed. PolyJet 3D printing uses liquid photopolymers that are dropped from a nozzle and cured layer-by-layer with ultraviolet (UV) light. Multi-material 3D printing can be readily realized in this method (but usually at a high cost). Direct laser writing (DLW) uses ultrafast laser pulses to induce nonlinear multi-photon absorption in a small laser spot and increase the resolution down to the sub-micrometer scale.

Fused deposition modeling (FDM) is based on material extrusion, where thermoplastic materials are melted and extruded through a nozzle. After extrusion, thermoplastic materials are solidified again and piled up to form successive object layers. It is widely used in either low-cost 3D printers or professional 3D printers, but it often results in low surface quality. In direct ink writing (DIW), inks flow through a syringe nozzle because of their low viscosity with applied shear stress. After printing, the structure maintains its 3D shape owing to the high viscosity of inks in the absence of shear stress. Metal powders and ceramic powders can be 3D-printed via selective laser sintering (SLS). The powder is sintered by a high-power laser and piled up layer-by-layer to form metal or ceramic 3D structures.

A few examples of 3D-printed components are shown in Figure 1: 3D-printed jet engine parts [7] (Figure 1a,b) and customized micro-lens (Figure 1c–e) [8–13].

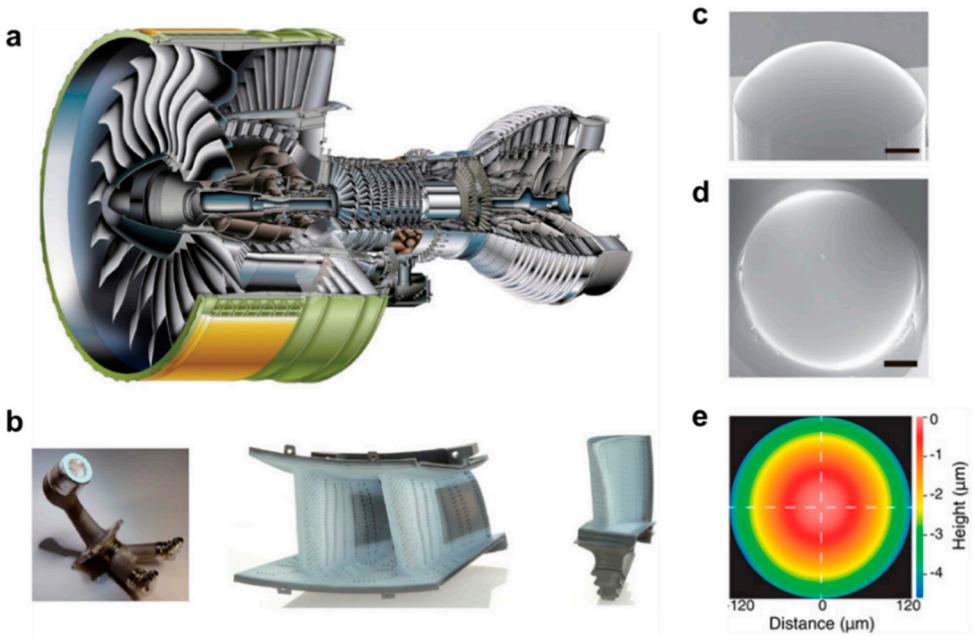

Figure 1. (**a**) Jet engine fabricated by 3D printing application; (**b**) 3D-printed jet engine parts. From left figure, there are fuel nozzle, high-pressure turbine nozzle, high-pressure turbine blade (Adapted from [7]. Copyright (2017) Elsevier); (**c**) Tilted view of SEM image of the 3D-printed optical lens using micro-stereolithography. Scale bar: 500 μm; (**d**) Top view of SEM image of the 3D-printed optical lens using micro-stereolithography. Scale bar: 500 μm; (**e**) Measured surface profile of the 3D-printed optical lens (Adapted from [13]. Copyright (2020) John Wiley & Sons).

Four-dimensional (4D) printing adds active, responsive functions to 3D-printed structures. The 4D printing concept was first introduced by S. Tibbits et al. in 2013 [14,15]. They demonstrated a 3D-printed rod structure that automatically transformed into a predesigned 3D geometry when immersed in water. Four-dimensional printing is often realized by printing smart materials, such as liquid crystal elastomers (LCE) [16–18], hydrogels [19–21], and shape memory polymers (SMP) [22–24]. Such structures can respond to environmental stimuli. In this sense, 4D-printed structures are also called programmable matter, where a response can be programmed into materials via structural and compositional design. In 4D printing, 3D-printed structures can be transformed in shape in response to external stimuli, such as heat [25], water [26], light [27,28], and pH [29].

Figure 3 shows several examples for 4D printing of smart materials. Figure 3a shows a 4D-printed hemispherical shell, made of LCE [30]. Owing to the reversible arrangement of liquid crystal molecules at different temperatures, shape morphing occurs in a pre-determined way. Figure 3b shows a gripper made of hydrogels [31]. Due to different swelling ratios between upper and lower layers, it can be bent when immersed in water. Figure 3c shows a self-bending structure upon light illumination [32].

A bilayer structure was fabricated using multi-color SMP printing, where blue and yellow SMP fibers were printed in a transparent elastomer matrix. Blue or red light can selectively heat yellow or blue SMP fibers, and thus the 3D-printed multicolor composite can be deformed into different shapes depending on light color. Four-dimensional printing could be useful for a wide range of potential applications, in actuators, switches, sensors, and deployable structures [33–35].

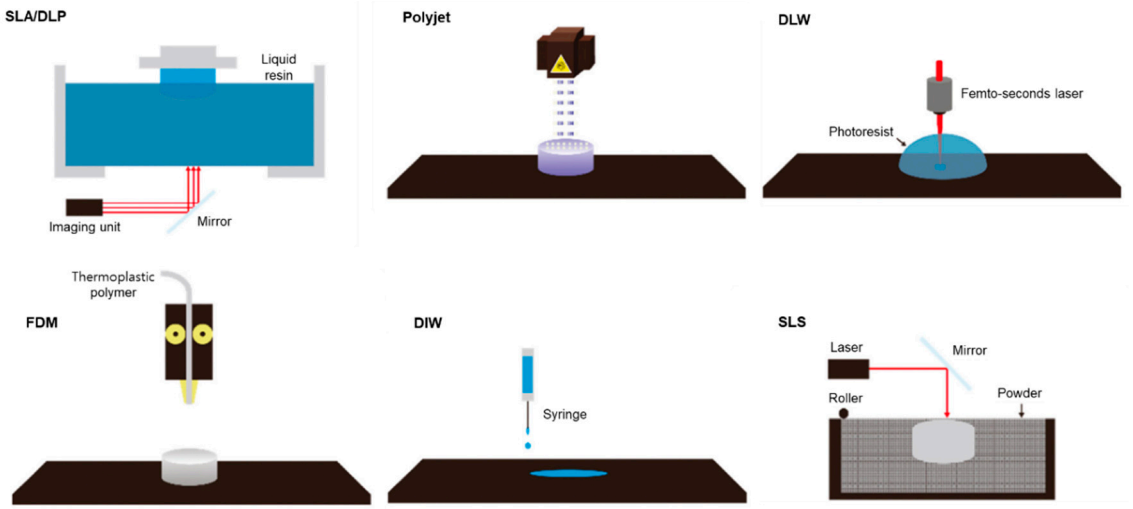

Figure 2. Schematic of various 3D printing processes: stereolithography (SLA)/digital light projector (DLP), PolyJet (or Material jetting), direct laser writing (DLW), fused deposition modeling (FDM), direct ink writing (DIW), selective laser sintering (SLS) (Adapted from [8]. Copyright (2020) De Gruyter).

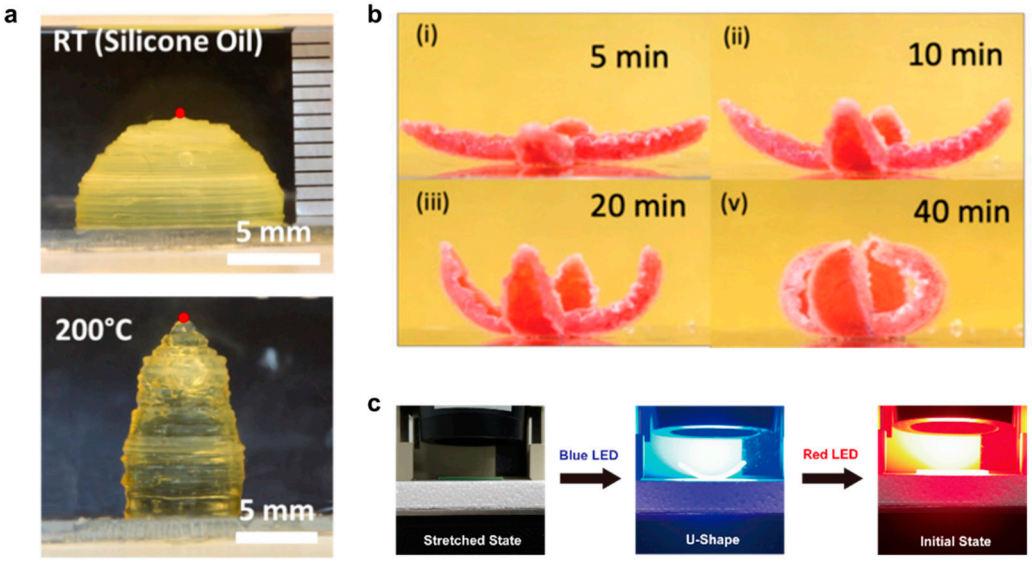

Figure 3. (**a**) Three-dimensional printed hemispherical structure using liquid crystal elastomers (LCE). Due to the anisotropic arrangement of the LC molecules, the structure expands in the z-direction at 200 °C (Adapted from [30]. Copyright (2017) ACS Publications); (**b**) Transformation of initially flat flower structure made by hydrogel bilayer blooming in the water. It takes 40 min to fully bloom (Adapted from [31]. Copyright (2019) John Wiley & Sons); (**c**) Transformation of initially flat stretched structure that bends on blue LED illumination and recover to the initial state on red LED illumination (Adapted from [32]. Copyright (2020) Nature Publishing Group).

Usually, 3D-printed components are static structures with fixed shapes and functions. One possible route to realize highly reconfigurable structures is to use mechanical multistability. It allows multiple stable configurations, and reversible switching between them is possible under proper mechanical

actions. Precisely controlled reconfiguration via multistability can bring many new breakthroughs to 3D printing. In fact, multistability exists even in nature. The Venus flytrap is one example (Figure 4a). The initially opened Venus flytrap leaf can abruptly snatch a worm by flipping the curvature of its inner structure. This abrupt motion, also called snap-through, originates from elastic bistability in the leaf [36].

Figure 4b shows the elastic potential energy diagram of such a bistable structure. It has two stable configurations that are separated by an energy barrier. The slope in the energy diagram indicates the force applied at a given displacement. Enough force should be applied to overcome this barrier and transform into the other stable state. Once passing the hill of the barrier, the bistable structure is deformed into another configuration automatically. In this way, bistable structures can induce a rapid, large-magnitude movement and thus can be used to simplify actuation and motion control. They can also be used as mechanical switches, because they do not require energy to maintain a stable state.

Bistability can be realized, for example, in strained bilayers and origami-based structures (Figure 4c) [37,38]. More complicated multistable structures can also be realized by combining basic units together (Figure 4d) [39]. These multistable structures can be engineered with many different design parameters. More advanced functionalities and enhanced controllability can also be obtained in 4D printing by adopting active materials in multistable structures. This could be useful for various smart actuators responding to the environmental stimuli.

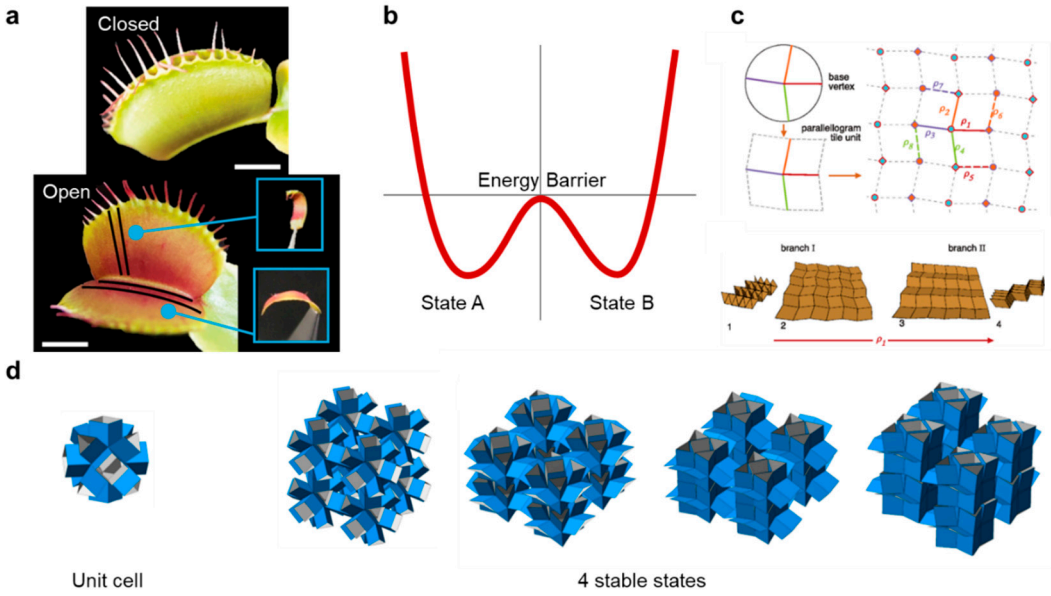

Figure 4. (**a**) Venus flytrap leaf in its closed and open states. Scale bar: 1 cm. (Adapted from [36]. Copyright (2020) John Wiley & Sons); (**b**) An example of the energy diagram of a bistable structure. There are two stable states corresponding to local energy minima. Once stimuli overcome the energy barrier, the bistable structure can snap-through to another stable state automatically; (**c**) Origami-based multistable structure. Different numbers of stable states can exist depending on design parameters (Adapted from [37]. Copyright (2015) American Physical Society); (**d**) Simulated results of cubic tessellation of a cuboctahedron unit cell. There are 4 stable states (Adapted from [39]. Copyright (2020) Nature Publishing Group).

In this short review, we briefly discuss recent developments in 3D and 4D printing of mechanical multistable structures. In Section 2, we introduce three different approaches for 3D printing of multistable structures: strained layers, compliant mechanisms, and mechanical metamaterials. In Section 3, we discuss 4D printing of multistable structures that could be applied to smart actuators. Lastly, in Section 4, we conclude with future prospects.

2. 3D Printing of Mechanical Multistable Structures

2.1. Strained Layer

One of the possible ways to realize mechanical multistability is the use of pre-strained layers [40–43]. In 3D printing, a residual thermal stress often remains after printing and it can cause a distortion of printed structures. Therefore, it is usually considered as a harmful effect and should be minimized. However, this residual stress can also be utilized in a clever way to create multistable structures. For example, Loukaides et al. fabricated bistable shell structures using selective laser sintering of metal powders [44]. A residual stress remains after the sintering process, and bistable shell structures can be formed (Figure 5a,b). The researchers printed cylindrical shells with varying curvatures. Figure 5a shows as-printed shapes, while Figure 5b shows another stable state. They also found that, when the pre-strain of the structure is too high, the structure becomes monostable (see the uppermost part in Figure 5a,b). They also confirmed this behavior with analytic modeling.

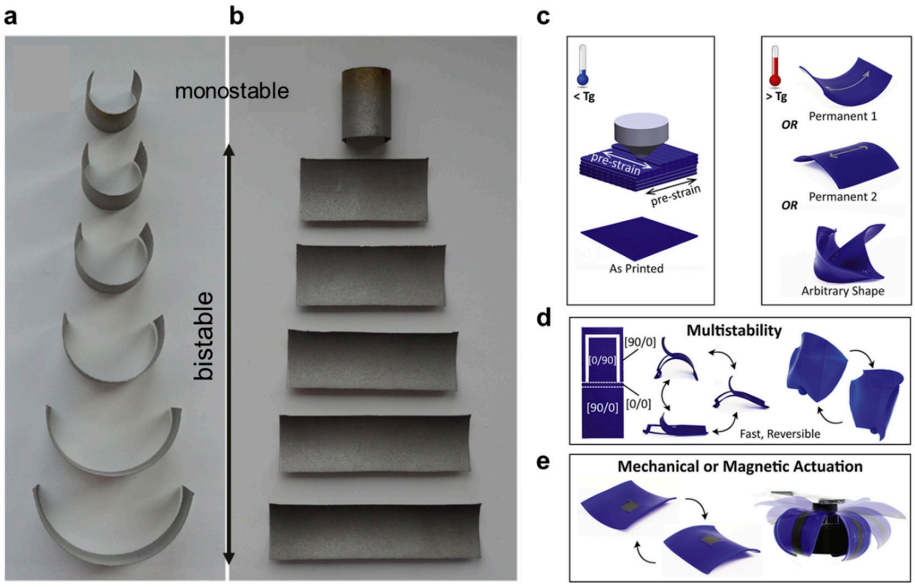

Figure 5. (**a**) As-printed shape of cylindrical shells (Radii 5,6,7,8,9,10 mm after removal from the build plate); (**b**) Another stable state of 3D-printed cylindrical shells (Adapted from [44]. Copyright (2019) IOP Publishing); (**c**) Morphing behavior of a 3D-printed bilayer structure. It remains flat below T_g. The initially flat structure can be activated to a bistable structure above T_g. It can maintain an arbitrary shape due to the shape memory polymer characteristic; (**d**) Bistability can be expanded to multistability with proper design: multistable chair structure and bistable Venus flytrap; (**e**) Bilayer structure and gripper design utilizing iron/polylatic acid (PLA) filaments. The gripper is activated by a magnet (Adapted from [45]. Copyright (2020) Elsevier).

Riley et al. reported a pre-strained bilayer using fused deposition modeling (FDM) [45]. FDM 3D printing can create pre-strain along the printing direction and this can be used to encode proper strains in printed structures. Figure 5c shows a schematic of the printed structure and its behavior. They printed a thin plate using polylatic acid (PLA). The lower half of the plate was printed in the x direction, while the upper half of the plate was printed in the y direction. The printed structure remains flat after printing due to the high stiffness of PLA at room temperature. However, above the glass transition temperature (T_g), the strain is released in the printed PLA plate. Then, a saddle-like bistable shape can be induced by the difference in the recovery direction between the upper and lower parts. This bistable shape can be flipped from upward to downward and vice versa. Above the T_g, the PLA plate can be deformed to arbitrary shapes too. When the structure is cooled down to room temperature, the temporary shape is fixed and does not show bistability. However, because of the shape memory

properties of PLA [25,46], when the structure is heated again above the T_g, it goes back to its permanent, bistable shape. In this way, temperature can be used as a switch for bistability. They expanded their idea to multistable structures (Figure 5d), and their 3D-printed bilayers were also applied to a gripper that operates under mechanical or magnetic actuation (Figure 5e).

2.2. Compliant Mechanism

A compliant mechanism is another possible method to realize mechanical multistable structures via 3D printing. A linear deformation of rigid materials can induce beam deflection in compliant mechanisms, and this can be used to induce multistable structures [47–52]. Beam deflection can occur in 3D-printed structures if a beam is thin enough; thus, 3D-printed compliant mechanisms can be used to create various multistable structures. For example, Jeong et al. fabricated global bistable structures via polyJet 3D printing [53]. By 3D printing ball and pin joints, they could realize twisting and rotating bistable structures without post assembly. Figure 6a shows the two stable states of the fabricated twisting bistable structure. Because two stable states have the same shape, the overall energy diagram is also symmetric (Figure 6b). Using pin joints, they also fabricated rotational bistable structures with two different boundary conditions: fixed-pinned and pinned-pinned boundaries (Figure 6c). The fixed-pinned boundary causes the beams in the stable state B to remain deformed. Because the deformed beams retain higher elastic energy, the overall energy diagram becomes asymmetric, as shown in Figure 6d (blue line). On the other hand, the pinned-pinned boundary allows the stable states A and B to have identical shapes. Therefore, the overall energy diagram remains symmetric in this case, as shown in Figure 6d (red line).

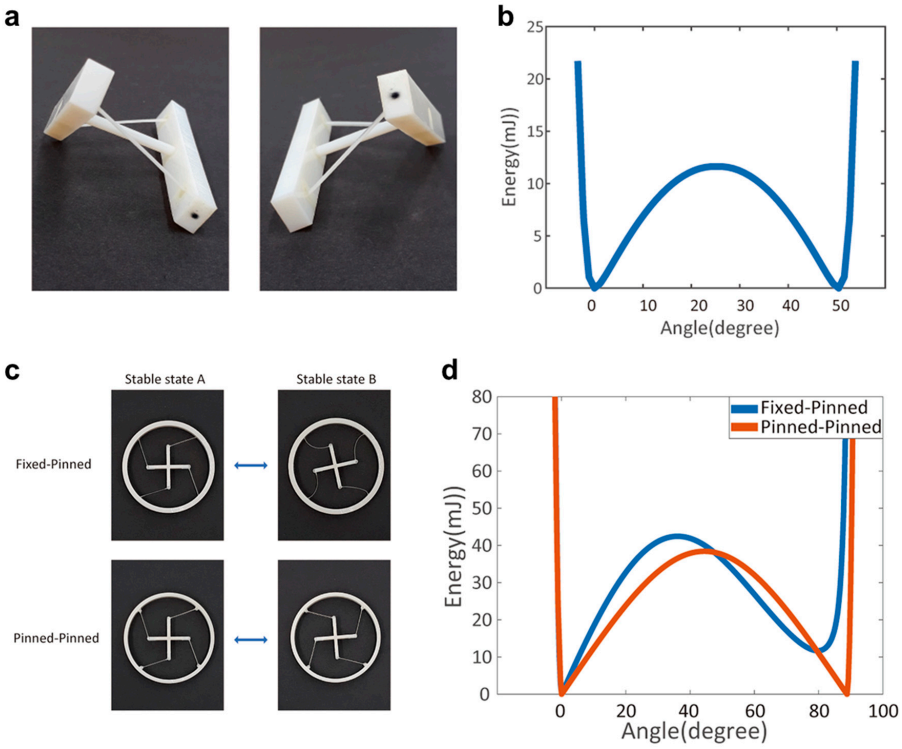

Figure 6. (**a**) Two stable states of a 3D-printed twisting bistable structure with ball joints. The black small dot is marked for eye tracing; (**b**) Simulated energy diagram of the twisting bistable structure. Due to the same shape of beams between two stable states, the energy diagram is also symmetric; (**c**) Two stable states of a 3D-printed rotational bistable structure with pin joints. When the inner cross is rotated clockwise while the outer ring is held fixed, the structure can transform from stable state A to another stable state B; (**d**) Energy diagram of the rotational bistable structure with different boundary conditions (Adapted from [53]. Copyright (2019) Nature Publishing Group).

Therefore, it is possible to adjust the overall energy diagram of the bistable structure and this can be used to tailor the mechanical response of printed structures. By adjusting the structural parameters or printing materials, it is possible to control the barrier height (i.e., the threshold energy for a shape change), the slope of the barrier (the force required for a shape change), and the amount of initial displacement to trigger a shape change. By connecting bistable structures, it is also possible to create multistable components. Therefore, this work demonstrates that 3D-printed multistable structures can be employed to realize highly controlled reconfiguration.

2.3. Mechanical Metamaterial

A bistable element can be used as a unit structure to construct multistable mechanical metamaterials. Properly designed mechanical metamaterials can show unusual mechanical properties such as negative Poisson's ratio, negative stiffness, energy trapping, etc. [54–60]. For example, constrained tilted elastic beams can be used to construct multistable mechanical metamaterials (Figure 7a–f). While an axially compressed elastic beam only has a single stable state (Figure 7a), a constrained tilted beam with fixed and roller boundary conditions can hold another deformed stable state (Figure 7b). The force-displacement curve in Figure 7b shows that it can be used as a bistable element. The difference between E_{in} and E_{out} in the force-displacement curve is the amount of trapped energy in this bistable element (Figure 7b).

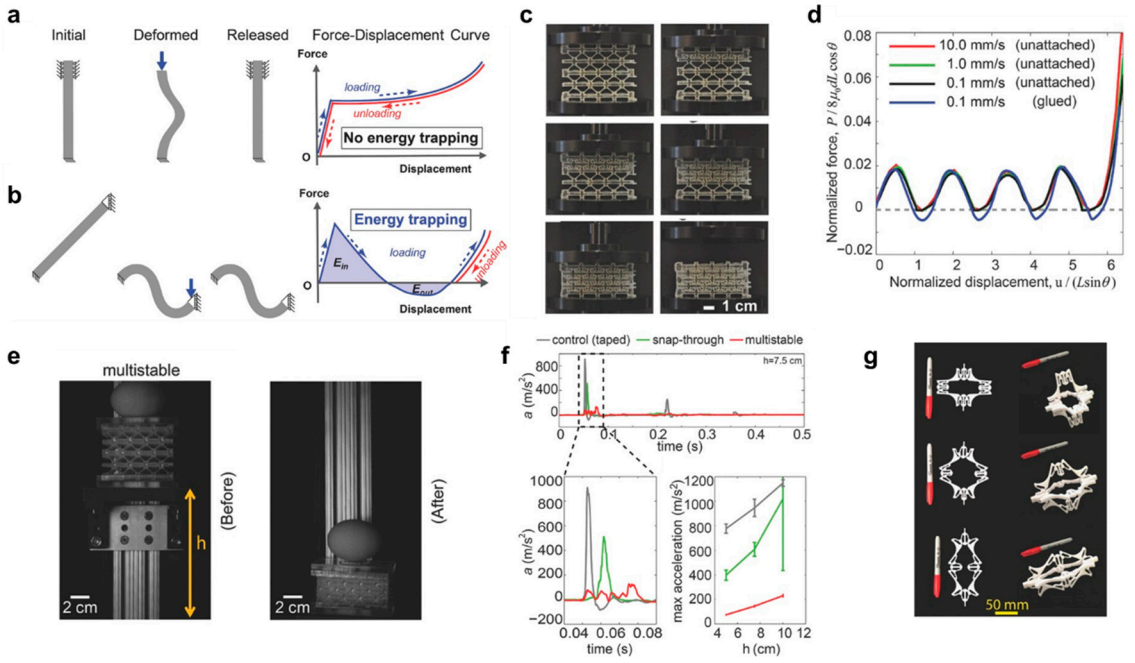

Figure 7. (**a**) An axially compressed elastic beam does not show bistability. It fully recovers to its initial state when unloaded; (**b**) An constrained tilted elastic beam can show bistability and energy trapping ($E_{in} - E_{out} > 0$). The deformed tilted elastic beam can recover to its initial state when enough energy is applied; (**c**) Compression test of 3D-printed multistable mechanical metamaterials. The sequentially deformed structure maintains a deformed state even after unloading; (**d**) Measured force and displacement graph. The overall deformation tendency is independent of loading conditions; (**e**) Demonstration of multistable mechanical metamaterials as an energy absorber. A raw egg mounted on the multistable mechanical metamaterial survived when dropped from a height of 12.5 cm; (**f**) Measured acceleration-time curve of three different cases. The control sample was taped so that all beams were intentionally collapsed before the drop test. The snap-through sample shows snap-through behavior but not energy trapping. Multistable mechanical metamaterials show a significant decrease in acceleration (Adapted from [57]. Copyright (2015) John Wiley & Sons); (**g**) Examples of 3D multistable mechanical metamaterials (Adapted from [60]. Copyright (2016) John Wiley & Sons).

Tilted beam bistable structures can be 3D-printed and have been used for multistable mechanical metamaterials. Shan et al. fabricated multistable energy trapping structures via direct ink writing [57]. They printed a 4 × 4 bistable structure using polydimethylsiloxane (PDMS), as shown in Figure 7c. When the fabricated multistable structure is uniaxially compressed, it undergoes snap-through four times because of four bistable layers along the compression direction. Figure 7d shows the measured force-displacement curve; four peaks correspond to the beginning of the snap-through. All peaks have the same magnitude because the structure consists of identical bistable layers. They also demonstrated that multistable metamaterials can be used as an energy absorber. As a proof-of-concept, they conducted a free-fall measurement of eggs. It is also compared to a control sample (taped) that does not show multistable behavior. An egg mounted on the multistable structure was unharmed and survived when it was dropped from the height (h) of 12.5 cm (Figure 7e). However, an egg on the control sample was broken because the control sample does not have the energy-absorbing capability. Figure 7f compares the acceleration-time graph for three cases: control sample, snap-through-only sample, and multistable sample. The control sample does not have an energy absorbing function and thus shows a high acceleration peak in a shortest time (blue curve). The snap-through-only sample shows a snap-through but without energy trapping. It still shows a reduced peak acceleration (green curve) compared to the control sample, due to the energy absorbing from the viscoelasticity of the material (not from the elastic energy trapping). The multistable sample shows a remarkable reduction in the peak amplitude because of the elastic energy trapping in mechanical metamaterials (red). Therefore, it could protect an egg during freefall.

Constrained tilted beams have also been used to control a snapping sequence in multistable metamaterials by 3D-printing imperfect unit cells [58] or adopting different materials on each layer [59]. Beam-based multistable metamaterials have been extended to 3D geometries too (Figure 7g) [60]. These studies demonstrate design flexibility available for multistable mechanical metamaterials.

3. 4D Printing of Multistable Structures

3.1. Heat-Responsive Structures

Four-dimensional printing can be implemented by printing smart materials. For example, SMPs can be employed as an active material in 4D printing. SMPs are smart materials that memorize a permanent shape. SMPs soften above the T_g and allow reshaping. This temporary shape can be fixed by cooling back to room temperature (also called thermo-mechanical programming), where SMPs exhibit significant stiffness. An SMP can be deformed into multiple, arbitrary temporary shapes and return to a permanent shape again upon a proper external stimulus (heat or light). Because SMPs can be readily printed in conventional 3D printers, SMPs have been widely considered for 4D printing research. By adopting SMPs in multistable structures, more advanced functionalities and enhanced controllability can be realized. Multistability can also help in increasing the load bearing capacity and the magnitude of actuation force.

For example, Tian Chen et al. devised a 3D-printed programmable actuator by combining a bistable structure with SMPs [35,61]. Figure 8a shows a schematic of their bistable structure (von Mises truss). Trusses are made of rigid materials, while beams and joints are based on compliant mechanisms. It possesses two stable states (retracted and extended states) which can be combined together to form a 3D geometry (Figure 8b). This bistable structure can be actuated by SMP strips. These strips can be deformed to a contracted shape above T_g. When cooled back to room temperature, SMP strips maintain the deformed shape (programmed state) (Figure 8c). Due to the SMP recovery, the deformed SMP strips return to the original state again above the T_g (activation). Figure 8d shows the bistable energy and force diagram. Once the SMP recovery force overcomes the energy barrier of the bistable structure, the unit actuator can snap-through to another stable state automatically. The recovery force can overcome the energy barrier by adjusting the thickness of SMP strips (Figure 8e).

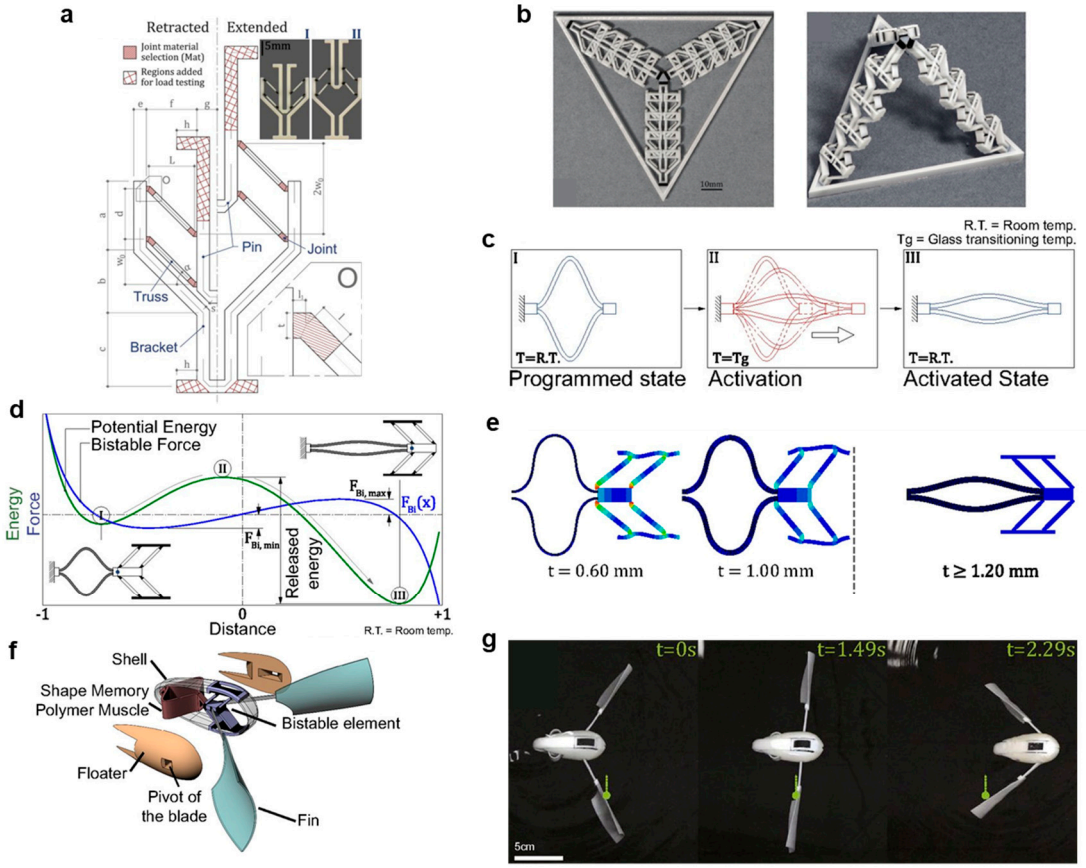

Figure 8. (**a**) Schematic of a 3D-printed von Mises bistable structure. The rigid bracket provides structural rigidity, while the flexible joints provide a rotational motion of the truss; (**b**) A 3D-printed bistable flat structure can be reconfigured to a 3D geometry via bistability (Adapted from [35]. Copyright (2017) Nature Publishing Group); (**c**) Programming and activation of SMP strips; (**d**) Bistable energy and force diagram with two stable states I and III; (**e**) Finite element (FE) simulation of SMP strips with varying thicknesses; (**f**) Schematic of an untethered swimming robot that enables a fin stroke in water; (**g**) Images of the swimming robot in warm water ($T > T_g$) at the different phases of activation (Adapted from [61]. Copyright (2018) National Academy of Sciences).

They also developed an autonomous actuator to realize soft, untethered robots for navigation and delivery [61]. Figure 8f shows a schematic of the proposed actuator. By attaching fins to the bistable structure, it can be actuated in water by a fin stroke. The large displacement of the bistable structure and the amplification of the actuation force helps the robot to swim in water. The programmed SMP actuator can return to its original state above T_g. When the SMP strip overcomes the energy barrier of the bistable structure, the robot can stroke its fins. Figure 8g shows images of the swimming robots. The robot can show sequential propulsion or directional motion by adjusting the thickness of SMP strips.

Jeong et al. used a rotational bistable structure (Figure 6) to fabricate a smart thermal actuator [62]. Multistable structures can simplify actuation and motion control without complicated control systems. Figure 9a shows the design schematic of the structure. They employ two different digital SMPs (rigid and rubbery ones) to enable large-angle, thermal actuation in a controlled manner. The rigid beam has a fixed-pinned boundary, while the rubbery one has a fixed-fixed boundary. Two rigid beams define the overall bistability, while the rubbery beams act as a control knob. Those multistable structures do not require heating in the programming stage and this significantly simplifies the actuation procedure (Figure 9b,c).

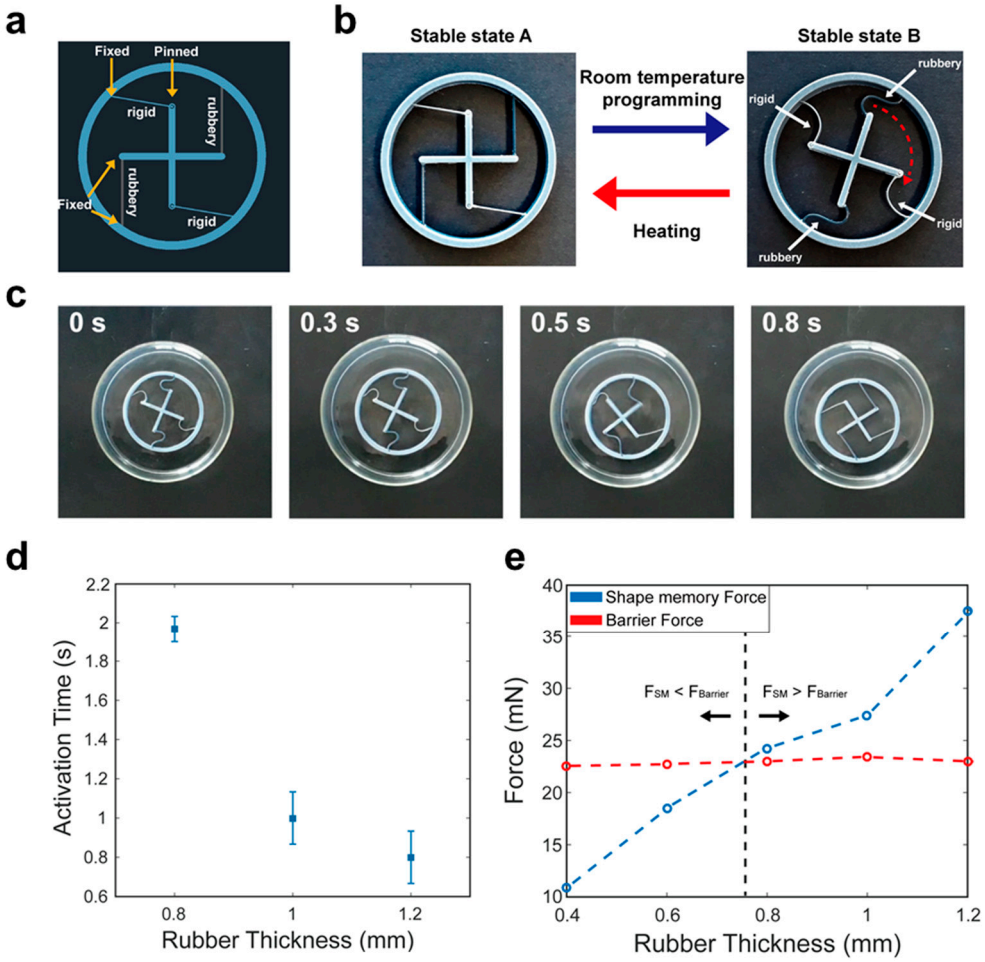

Figure 9. (**a**) Schematic of a rotational bistable structure that can be activated by heat: similar to Figure 6c but two fixed-pinned beams were replaced by fixed-fixed rubbery beams; (**b**) Operating procedure of the fabricated thermal actuator. It is possible to program the structure at room temperature. The rotated structure (stable state B) at room temperature returns to its original stable state A at 75 °C; (**c**) Images of the thermal actuator in 75 °C water. It returns to the initial stable state in 0.8 s; (**d**) Activation time of the thermal actuator for different rubbery beam thicknesses; (**e**) Comparison of the shape memory force and barrier force. Thermal actuation occurs when the shape memory force is larger than the barrier force (Adapted from [62]. Copyright (2019) John Wiley & Sons).

In their design, by adjusting the thickness of SMP beams, they could control a balance between the energy barrier and shape-memory force, and this enabled controlled thermal actuation. They could also control the activation time for thermal actuation; as the thickness of rubber SMP increases, the activation time decreases (Figure 9d). The researchers conducted a detailed analysis using finite element simulations and shape memory force measurements (Figure 9e). They also extended their bistable structures to quadristable ones. Thus, 4D-printed multistable structures could be useful for various smart and programmable actuators responding to the environmental stimuli.

3.2. Solvent-Responsive Structures

Jiang et al. demonstrated logic operation using stimuli-responsive bistable structures [63]. The bistable structures were fabricated via the direct ink writing (DIW) of glass fiber (GF) embedded polydimethylsiloxane (PDMS). The GF in a PDMS network can be aligned along the extrusion direction. PDMS can absorb non-polar solvents such as toluene. Aligned GFs prevent PDMS from swelling along the aligned direction, so that anisotropic swelling can be achieved. The schematic of the bistable element is shown in Figure 10a. The bistable structure consists of two beams with fixed and roller boundary

conditions (same as Figure 7c). In this configuration, the structure can have monostability or bistability upon geometrical parameters. They kept the tilted angle as 45°, while they changed the slenderness ratio (w/L). There exists a certain slenderness ratio that divides monostability and bistability, which is called a bifurcation point. Figure 10b shows the energy diagram of the monostable and bistable structures. The energy of the monostable structure monotonically increases, while the energy of the bistable structure has a local minimum that corresponds to a second stable state. Figure 10c shows the geometric phase diagram together with the image of printed structures. Due to the anisotropic swelling, the slenderness ratio of the PDMS-GF bistable structure can be increased when it is immersed in toluene. Therefore, bistability can turn into monostability (see the blue curve). At the transition point, the transition speed is found to be very fast (less than 0.01 s).

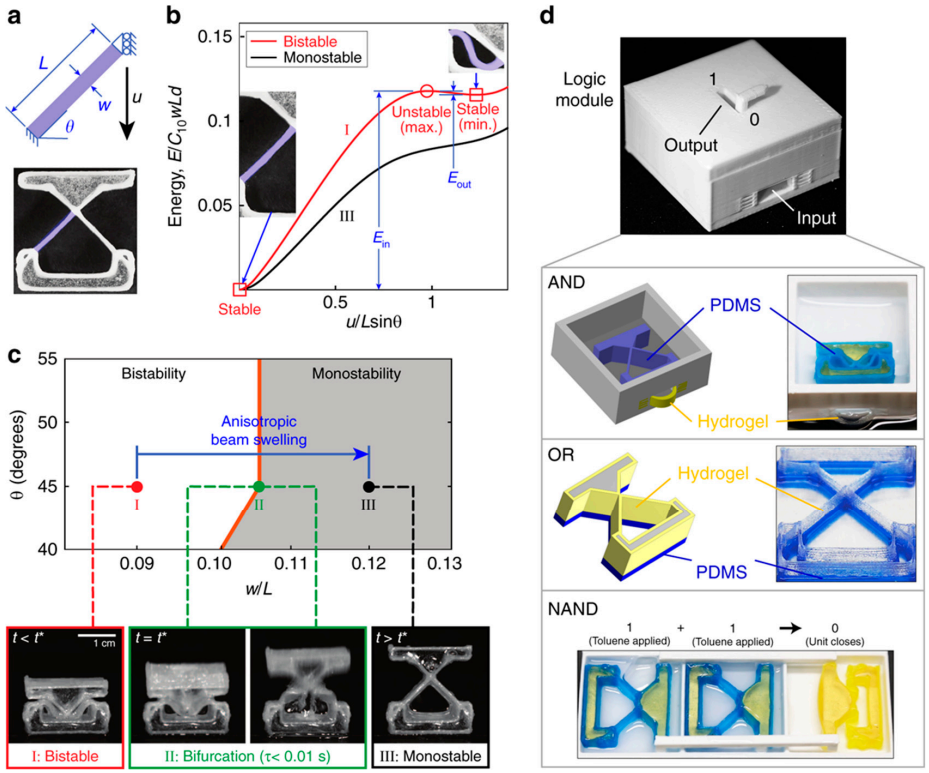

Figure 10. (**a**) Schematic and image of a bistable structure; (**b**) Energy-displacement curve of the bistable structure (I) and the monostable structure (III). The inset images are configuration of beams at each stable state; (**c**) The initially bistable structure (I) can transform into a monostable structure (III) due to anisotropic beam swelling. There is a transition at the bifurcation point (II). Representative images are also shown at the bottom for the bistable state (red), the bifurcation point when actuation occurs (green), and the monostable state (black); (**d**) Logic gates fabricated by combining glass fiber embedded polydimethylsiloxane (PDMS-GF) (activated by toluene) and hydgrogel-nanofibrillated cellulose (NFC) (activated by water) bistable structures (Adapted from [63]. Copyright (2019) Nature Publishing Group).

They also fabricated a bistable structure using hydrogels embedded with nanofibrillated cellulose (NFC). The NFC filler prevents hydrogels from isotropic swelling in water. The researchers fabricated a proof-of-concept module for logic operation by selectively activating bistable elements in a polar or non-polar solvent (Figure 10d). Combining the PDMS-GF (activated by toluene) and hydrogel-NFC (activated by water) bistable elements together, they could demonstrate AND, OR, and NAND logic gates. The AND gate consists of a hydrogel valve and a PDMS-GF bistable unit (both water and toluene required). The OR gate consists of a combined hydrogel-NFC and PDMS-GF bistable unit (either water or toluene required). The NAND gate is constructed by connecting two input bistable units to one

output unit. The connected input and output parts can be activated by applying toluene to both input units. In this way, an initially opened output unit can be closed. They could also control the actuation time by adjusting the slenderness ratio. This actuator is scale-independent, and thus it can be modified properly for other applications including soft robotics, biomedical devices, and deployable structures.

Other responsive materials can also be used for multistable structures. For example, Figure 5e shows a bistable bilayer structure that was 3D-printed with iron/PLA filaments. The gripper action can be triggered by an external magnetic field above the T_g. A variety of smart and programmable actuators can be realized via 4D-printed multistable structures, in response to various environmental stimuli, such as heat, light, moisture, pH level, and electric/magnetic fields.

4. Conclusions and Future Prospects

Lastly, in this section, we introduce a few more recent works that utilized multistable structures for actuation and reconfiguration. Although they are not yet fully 3D-printed, these works provide interesting perspectives on multistability. As multi-material 3D-printing technologies are developing rapidly, we expect that similar structures could also be realized via 3D printing in the near future.

Tang et al. [64] developed a bistable spine mechanism for soft-legged robots (Figure 11a–c). They demonstrated high-speed yet energy-efficient spine flexion and extension with insights from quadrupedal mammals. High-speed locomotion requires the rapid storage and release of large mechanical energy as well as high force output. However, most soft robots have slow response time and low energy exertion due to material softness and structural compliance. Motivated by galloping cheetahs, a bistable hybrid soft bending actuator was proposed to overcome this limitation. It was built by joining 3D-printed, spring-based bistable linkages ("spine") to soft pneumatic bending actuators ("muscles") (Figure 11a,b). They demonstrated a high-speed soft crawler (Figure 11c) using a bistable spine mechanism, which is over 2.5 times faster and still requires less input energy for operation than high energy density dielectric crawlers.

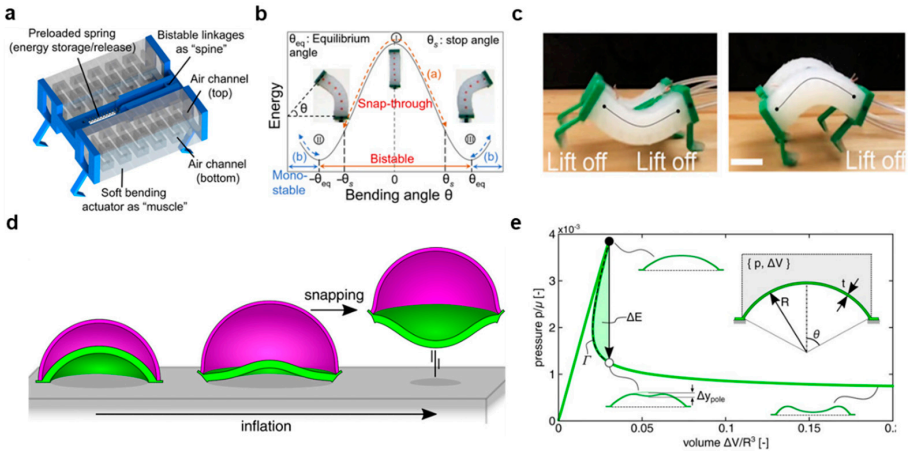

Figure 11. (**a**) Schematic of a bistable hybrid soft bending actuator (BH-SBA). It consists of two soft air-bending actuators, 3D-printed bistable linkages, and a preloaded spring that stores potential energy and releases when the air channel is pressurized; (**b**) Energy diagram of the bistable actuator. The axially pre-tensioned spring makes maximum energy at the zero bending angle. As the spring releases the energy with bending, the whole energy decreases and finally reaches the energy minima (θ_{eq}); (**c**) Fabricated bio-inspired crawler with the spine actuation. The spine bends upward to store energy and downward to release energy (Adapted from [64]. Copyright (2020) AAAS); (**d**) Fabricated soft actuator that can jump when the inner spherical cap flips downward during inflation; (**e**) Pressure-volume curve of the soft actuator. Isochoric snapping can occur and the inner spherical cap flips downward. During the flipping, the volume of cavity is maintained but the pressure drops. ΔE is the amount of energy releasing (Adapted from [65]. Copyright (2020) AAAS).

Gorissen et al. introduced a fluidic soft actuator utilizing the snapping mechanism of a spherical cap, which turns a slow input signal into a remarkably swift jump (Figure 11d,e) [65]. The fluidic soft actuator consists of elastomeric inner and outer spherical caps that are connected at their bottom to form a cavity, where incompressible fluid can flow. Isochoric snapping instability leads to a sudden release of substantial elastic energy, the amount of which is given by the enclosed domain between the upper limit point and the equivalent isochoric point on the lower in the pressure-volume curve. A rapid inversion of the inner cap occurs, resulting in ultimately jumping. The amount of energy release can be modulated by the geometry, stiffness, and the boundary conditions of the caps, so that the response of the actuators can be enhanced even though the inflation rate is tardy.

Multistability can also be utilized to enable reconfigurable microelectronic devices. For example, Fu et al. fabricated morphable 3D mesostructures and microelectronic devices using multistable structures based on pre-strained elastomers and 2D precursors [66]. Reversible reconfiguration is obtained by strategically organizing the time sequence of the strain release and by engineering precursor designs. They demonstrated more than 20 examples for MOSFET, LED, and RF circuit integrated devices.

In this paper, we have briefly introduced recent developments in 3D and 4D printing of mechanical multistable structures. We first discussed three representative approaches in 3D printing of multistable structures. Then, we presented 4D printing of multistable structures designed for smart actuators and soft robots. Mechanical multistable structures have characteristics superior to conventional structures in several ways. They can allow reconfigurable shapes and remain in a stable state unless an external stimulus overcomes the structure's energy barrier. Moreover, mechanical multistable structures can enable more accurate motion control because motion can be directed to energetically favored stable states. Furthermore, it is possible to activate structures more rapidly via snap-through transitions. They can also show stimuli-active responses by adopting active materials into multistable structures. Therefore, multistable structures are expected to play an important role in 3D and 4D printing applications.

Three-dimensional printing has also been considered for biomedical applications, such as scaffold [3–6], splint [67], and stent [68]. Stimuli-responsive and biocompatible materials (such as hydrogels) were also 3D-printed for drug delivery [69]. Various 4D printing techniques could be helpful for releasing drugs at a precise target position. With the development of biocompatible printing materials, 4D printing is becoming attractive to bioprinting and biomedical applications [70–72]. Moreover, 4D bioprinting has an advantage in constructing 3D complex tissue structures based on responsive materials, which can reconstruct or alter their function upon external stimuli. In addition, 4D bioprinting can generate printed cell populations with programmable scaffold structures. It could be applicable to tissue engineering, such as dynamic tissue healing and regeneration for the injured human body. Multi-stable structures can be potentially useful for these biomedical applications too, because they can provide large-magnitude, highly controllable shape changes. Various actuation and reconfiguration schemes can be considered for these applications.

Table 1 summarizes the multistable 4D printing schemes considered in this paper. It helps in understanding the current status and challenges for multistable 4D printing. By adopting smart materials in multistable structures, more advanced functionalities and enhanced controllability can be realized. Multistability could also help in increasing the magnitude of actuation force as well as the load bearing capacity.

We also expect that the concept of 3D-printed multistable structures which we have discussed in this article could be extended to the micrometer scale too. Sub-micrometer patterns can be created using direct laser writing with two photon absorption [73–76]. In addition, stimuli-responsive materials can be utilized in direct laser writing too [8,77–80]. This could lead to interesting research opportunities for micrometer-scale multistable structures, including applications in biomedical devices. These microscale multistable structures can be actuated by various external stimuli (heat, light, magnetic fields, etc.),

and this could be a very interesting way to realize more complicated functions at the micrometer scale. Therefore, we think there are abundant new opportunities to explore further.

Table 1. Summary of multistable 4D printing schemes.

Name of the Scheme	Basic Cell and Principle	Key Feature	Printing Materials for Actuation	Actuation Stimulus	Ref.
Soft actuator	Bistable Von Mises truss (Figure 8a)	Sequential swimming in water	SMP	Heat	[61]
Rotational thermal actuator	Rotational compliant mechanism (Figures 6c and 9a)	Room temperature programming	SMP	Heat	[62]
Logic operator	Constrained tilted elastic beam (Figures 7c and 10a)	Logic operation with expandable bistable elements	PDMS, Hydrogel	Solvent (toluene, water)	[63]
Gripper	Strained bilayer (Figure 5e)	Gripping via thermomechanical and magnetic actuation	Iron/PLA	Magnetic field	[45]

Author Contributions: All authors contributed to manuscript writing. All authors have read and agreed to the published version of the manuscript.

Funding: This research was funded by National Research Foundation (NRF) of Korea (2018R1E1A2A02086050,) and Ulsan National Institute of Science and Technology through the Development of 3D Printing-Based Smart Manufacturing Core Technology Research Fund under grant 1.200069.01.

Conflicts of Interest: The authors declare no conflict of interest.

References

1. Gao, W.; Zhang, Y.; Ramanujan, D.; Ramani, K.; Chen, Y.; Williams, C.B.; Wang, C.C.; Shin, Y.C.; Zhang, S.; Zavattieri, P.D. The status, challenges, and future of additive manufacturing in engineering. *Comput.-Aided Des.* **2015**, *69*, 65–89. [CrossRef]
2. Bose, S.; Vahabzadeh, S.; Bandyopadhyay, A. Bone tissue engineering using 3D printing. *Mater. Today* **2013**, *16*, 496–504. [CrossRef]
3. Ma, H.; Feng, C.; Chang, J.; Wu, C. 3D-printed bioceramic scaffolds: From bone tissue engineering to tumor therapy. *Acta Biomater.* **2018**, *79*, 37–59. [CrossRef] [PubMed]
4. Wang, J.; Yang, M.; Zhu, Y.; Wang, L.; Tomsia, A.P.; Mao, C. Phage nanofibers induce vascularized osteogenesis in 3D printed bone scaffolds. *Adv. Mater.* **2014**, *26*, 4961–4966. [CrossRef]
5. Yan, Y.; Chen, H.; Zhang, H.; Guo, C.; Yang, K.; Chen, K.; Cheng, R.; Qian, N.; Sandler, N.; Zhang, Y.S. Vascularized 3D printed scaffolds for promoting bone regeneration. *Biomaterials* **2019**, *190*, 97–110. [CrossRef]
6. Hull, C.W. Apparatus for Production of Three-Dimensional Objects by Stereolithography. U.S. Patent US4575330A, 8 August 1984.
7. Han, P.L. Additive Design and Manufacturing of Jet Engine Parts. *Engineering* **2017**, *3*, 648–652. [CrossRef]
8. Jeong, H.Y.; Lee, E.; An, S.C.; Lim, Y.; Jun, Y.C. 3D and 4D printing for optics and metaphotonics. *Nanophotonics* **2020**, *9*, 1139–1160. [CrossRef]
9. Suszek, J.; Siemion, A.; Bieda, M.S.; Błocki, N.; Coquillat, D.; Cywiński, G.; Czerwińska, E.; Doch, M.; Kowalczyk, A.; Palka, N. 3-D-printed flat optics for THz linear scanners. *IEEE Trans. Terahertz Sci. Technol.* **2015**, *5*, 314–316. [CrossRef]
10. Udofia, E.N.; Zhou, W. 3D Printed optics with a soft and stretchable optical material. *Addit. Manuf.* **2020**, *31*, 100912.
11. López-Valdeolivas, M.; Liu, D.; Broer, D.J.; Sánchez-Somolinos, C. 4D printed actuators with soft-robotic functions. *Macromol. Rapid Commun.* **2018**, *39*, 1700710. [CrossRef]
12. Vaidya, N.; Solgaard, O. 3D printed optics with nanometer scale surface roughness. *Microsyst. Nanoeng.* **2018**, *4*, 18. [CrossRef]
13. Shao, G.; Hai, R.; Sun, C. 3D Printing Customized Optical Lens in Minutes. *Adv. Opt. Mater.* **2020**, *8*, 1901646. [CrossRef]

14. Tibbits, S. The emergence of "4D printing". *TED Conf.* **2013**.
15. Tibbits, S. 4D printing: Multi-material shape change. *Archit. Des.* **2014**, *84*, 116–121. [CrossRef]
16. Yuan, C.; Roach, D.J.; Dunn, C.K.; Mu, Q.; Kuang, X.; Yakacki, C.M.; Wang, T.; Yu, K.; Qi, H.J. 3D printed reversible shape changing soft actuators assisted by liquid crystal elastomers. *Soft Matter* **2017**, *13*, 5558–5568. [CrossRef]
17. Saed, M.O.; Ambulo, C.P.; Kim, H.; De, R.; Raval, V.; Searles, K.; Siddiqui, D.A.; Cue, J.M.O.; Stefan, M.C.; Shankar, M.R. Molecularly-Engineered, 4D-Printed Liquid Crystal Elastomer Actuators. *Adv. Funct. Mater.* **2019**, *29*, 1806412. [CrossRef]
18. Ahn, C.; Liang, X.; Cai, S. Bioinspired design of light-powered crawling, squeezing, and jumping untethered soft robot. *Adv. Mater. Technol.* **2019**, *4*, 1900185. [CrossRef]
19. Bakarich, S.E.; Gorkin, R., III; Panhuis, M.I.H.; Spinks, G.M. 4D printing with mechanically robust, thermally actuating hydrogels. *Macromol. Rapid Commun.* **2015**, *36*, 1211–1217. [CrossRef]
20. Gladman, A.S.; Matsumoto, E.A.; Nuzzo, R.G.; Mahadevan, L.; Lewis, J.A. Biomimetic 4D printing. *Nat. Mater.* **2016**, *15*, 413–418. [CrossRef]
21. Huang, L.; Jiang, R.; Wu, J.; Song, J.; Bai, H.; Li, B.; Zhao, Q.; Xie, T. Ultrafast digital printing toward 4D shape changing materials. *Adv. Mater.* **2017**, *29*, 1605390. [CrossRef]
22. Ge, Q.; Qi, H.J.; Dunn, M.L. Active materials by four-dimension printing. *Appl. Phys. Lett.* **2013**, *103*, 131901. [CrossRef]
23. Wu, J.; Yuan, C.; Ding, Z.; Isakov, M.; Mao, Y.; Wang, T.; Dunn, M.L.; Qi, H.J. Multi-shape active composites by 3D printing of digital shape memory polymers. *Sci. Rep.* **2016**, *6*, 24224. [CrossRef]
24. Ding, Z.; Yuan, C.; Peng, X.; Wang, T.; Qi, H.J.; Dunn, M.L. Direct 4D printing via active composite materials. *Sci. Adv.* **2017**, *3*, e1602890. [CrossRef]
25. Zhang, Q.; Yan, D.; Zhang, K.; Hu, G. Pattern transformation of heat-shrinkable polymer by three-dimensional (3D) printing technique. *Sci. Rep.* **2015**, *5*, 8936. [CrossRef]
26. Raviv, D.; Zhao, W.; McKnelly, C.; Papadopoulou, A.; Kadambi, A.; Shi, B.; Hirsch, S.; Dikovsky, D.; Zyracki, M.; Olguin, C. Active printed materials for complex self-evolving deformations. *Sci. Rep.* **2014**, *4*, 7422. [CrossRef] [PubMed]
27. Kuksenok, O.; Balazs, A.C. Stimuli-responsive behavior of composites integrating thermo-responsive gels with photo-responsive fibers. *Mater. Horiz.* **2016**, *3*, 53–62. [CrossRef]
28. Yang, H.; Leow, W.R.; Wang, T.; Wang, J.; Yu, J.; He, K.; Qi, D.; Wan, C.; Chen, X. 3D printed photoresponsive devices based on shape memory composites. *Adv. Mater.* **2017**, *29*, 1701627. [CrossRef] [PubMed]
29. Nadgorny, M.; Xiao, Z.; Chen, C.; Connal, L.A. Three-dimensional printing of pH-responsive and functional polymers on an affordable desktop printer. *ACS Appl. Mater. Interfaces* **2016**, *8*, 28946–28954. [CrossRef] [PubMed]
30. Ambulo, C.P.; Burroughs, J.J.; Boothby, J.M.; Kim, H.; Shankar, M.R.; Ware, T.H. Four-dimensional printing of liquid crystal elastomers. *ACS Appl. Mater. Interfaces* **2017**, *9*, 37332–37339. [CrossRef] [PubMed]
31. Shiblee, M.N.I.; Ahmed, K.; Kawakami, M.; Furukawa, H. 4D Printing of Shape-Memory Hydrogels for Soft-Robotic Functions. *Adv. Mater. Technol.* **2019**, *4*, 1900071. [CrossRef]
32. Jeong, H.Y.; Woo, B.H.; Kim, N.; Jun, Y.C. Multicolor 4D printing of shape-memory polymers for light-induced selective heating and remote actuation. *Sci. Rep.* **2020**, *10*, 6258. [CrossRef]
33. Yang, C.; Boorugu, M.; Dopp, A.; Ren, J.; Martin, R.; Han, D.; Choi, W.; Lee, H. 4D printing reconfigurable, deployable and mechanically tunable metamaterials. *Mater. Horiz.* **2019**, *6*, 1244–1250. [CrossRef]
34. Akbari, S.; Sakhaei, A.H.; Kowsari, K.; Yang, B.; Serjouei, A.; Yuanfang, Z.; Ge, Q. Enhanced multimaterial 4D printing with active hinges. *Smart Mater. Struct.* **2018**, *27*, 065027. [CrossRef]
35. Chen, T.; Mueller, J.; Shea, K. Integrated design and simulation of tunable, multi-state structures fabricated monolithically with multi-material 3D printing. *Sci. Rep.* **2017**, *7*, 45671. [CrossRef] [PubMed]
36. Lunni, D.; Cianchetti, M.; Filippeschi, C.; Sinibaldi, E.; Mazzolai, B. Plant-Inspired Soft Bistable Structures Based on Hygroscopic Electrospun Nanofibers. *Adv. Mater. Interfaces* **2020**, *7*, 8. [CrossRef]
37. Waitukaitis, S.; Menaut, R.; Chen, B.G.-g.; van Hecke, M. Origami multistability: From single vertices to metasheets. *Phys. Rev. Lett.* **2015**, *114*, 055503. [CrossRef]
38. Dudte, L.H.; Vouga, E.; Tachi, T.; Mahadevan, L. Programming curvature using origami tessellations. *Nat. Mater.* **2016**, *15*, 583–588. [CrossRef]

39. Iniguez-Rabago, A.; Li, Y.; Overvelde, J.T. Exploring multistability in prismatic metamaterials through local actuation. *Nat. Commun.* **2019**, *10*, 5577. [CrossRef]
40. Kebadze, E.; Guest, S.; Pellegrino, S. Bistable prestressed shell structures. *Int. J. Solids Struct.* **2004**, *41*, 2801–2820. [CrossRef]
41. Wang, B.; Ge, C.; Fancey, K.S. Snap-through behaviour of a bistable structure based on viscoelastically generated prestress. *Compos. B Eng.* **2017**, *114*, 23–33. [CrossRef]
42. Jiang, X.; Pezzulla, M.; Shao, H.; Ghosh, T.K.; Holmes, D.P. Snapping of bistable, prestressed cylindrical shells. *EPL* **2018**, *122*, 64003. [CrossRef]
43. Hu, N.; Han, X.; Huang, S.; Grover, H.; Yu, X.; Zhang, L.; Trase, I.; Zhang, J.; Zhang, L.; Dong, L. Edge effect of strained bilayer nanofilms for tunable multistability and actuation. *Nanoscale* **2017**, *9*, 2958–2962. [CrossRef]
44. Loukaides, E.G.; Lewis, R.W.; Bowen, C.R. Additive manufacture of multistable structures. *Smart Mater. Struct.* **2019**, *28*, 02LT02. [CrossRef]
45. Riley, K.S.; Ang, K.J.; Martin, K.A.; Chan, W.K.; Faber, J.A.; Arrieta, A.F. Encoding multiple permanent shapes in 3D printed structures. *Mater. Des.* **2020**, *194*, 108888. [CrossRef]
46. An, S.C.; Lee, E.; Lee, C.H.; Jeong, H.Y.; Kwon, T.S.; Lee, J.H.; Jun, Y.C. Sharp Fano Resonance and Spectral Collapse in Stimuli-Responsive Photonic Structures. *Adv. Opt. Mater.* **2019**, *7*, 1801206. [CrossRef]
47. Hussein, H.; Younis, M.I. Analytical study of the snap-through and bistability of beams with arbitrarily initial shape. *J. Mech. Robot.* **2020**, *12*, 041001. [CrossRef]
48. Ma, F.; Chen, G.; Wang, H. Large-Stroke Constant-Force Mechanisms Utilizing Second Buckling Mode of Flexible Beams: Evaluation Metrics and Design Approach. *J. Mech. Des.* **2020**, *142*, 103303. [CrossRef]
49. Chen, Q.; Zhang, X.; Zhang, H.; Zhu, B.; Chen, B. Topology optimization of bistable mechanisms with maximized differences between switching forces in forward and backward direction. *Mech. Mach. Theory* **2019**, *139*, 131–143. [CrossRef]
50. Chen, G.; Ma, F.; Hao, G.; Zhu, W. Modeling large deflections of initially curved beams in compliant mechanisms using chained beam constraint model. *J. Mech. Robot.* **2019**, *11*, 011002. [CrossRef]
51. Chen, G.; Han, Q.; Jin, K. A Fully Compliant Tristable Mechanism Employing Both Tensural and Compresural Segments. *J. Mech. Robot.* **2020**, *12*, 011003. [CrossRef]
52. Chen, G.; Gou, Y.; Zhang, A. Synthesis of compliant multistable mechanisms through use of a single bistable mechanism. *J. Mech. Des.* **2011**, *133*, 081007. [CrossRef]
53. Jeong, H.Y.; An, S.-C.; Seo, I.C.; Lee, E.; Ha, S.; Kim, N.; Jun, Y.C. 3D printing of twisting and rotational bistable structures with tuning elements. *Sci. Rep.* **2019**, *9*, 324. [CrossRef]
54. Yang, H.; Ma, L. Angle-Dependent Transitions Between Structural Bistability and Multistability. *Adv. Eng. Mater.* **2020**, *22*, 1900871. [CrossRef]
55. Yang, H.; Ma, L. Multi-stable mechanical metamaterials with shape-reconfiguration and zero Poisson's ratio. *Mater. Des.* **2018**, *152*, 181–190. [CrossRef]
56. Yang, H.; Ma, L. Multi-stable mechanical metamaterials by elastic buckling instability. *J. Mater. Sci.* **2019**, *54*, 3509–3526. [CrossRef]
57. Shan, S.; Kang, S.H.; Raney, J.R.; Wang, P.; Fang, L.; Candido, F.; Lewis, J.A.; Bertoldi, K. Multistable architected materials for trapping elastic strain energy. *Adv. Mater.* **2015**, *27*, 4296–4301. [CrossRef]
58. Che, K.; Yuan, C.; Wu, J.; Qi, H.J.; Meaud, J. Three-dimensional-printed multistable mechanical metamaterials with a deterministic deformation sequence. *J. Appl. Mech.* **2017**, *84*, 011004. [CrossRef]
59. Che, K.; Yuan, C.; Qi, H.J.; Meaud, J. Viscoelastic multistable architected materials with temperature-dependent snapping sequence. *Soft Matter* **2018**, *14*, 2492–2499. [CrossRef]
60. Haghpanah, B.; Salari-Sharif, L.; Pourrajab, P.; Hopkins, J.; Valdevit, L. Multistable shape-reconfigurable architected materials. *Adv. Mater.* **2016**, *28*, 7915–7920. [CrossRef]
61. Chen, T.; Bilal, O.R.; Shea, K.; Daraio, C. Harnessing bistability for directional propulsion of soft, untethered robots. *Proc. Natl. Acad. Sci. USA* **2018**, *115*, 5698–5702. [CrossRef]
62. Jeong, H.Y.; Lee, E.; Ha, S.; Kim, N.; Jun, Y.C. Multistable thermal actuators via multimaterial 4D printing. *Adv. Mater. Technol.* **2019**, *4*, 1800495. [CrossRef]
63. Jiang, Y.; Korpas, L.M.; Raney, J.R. Bifurcation-based embodied logic and autonomous actuation. *Nat. Commun.* **2019**, *10*, 128. [CrossRef] [PubMed]

64. Tang, Y.; Chi, Y.; Sun, J.; Huang, T.-H.; Maghsoudi, O.H.; Spence, A.; Zhao, J.; Su, H.; Yin, J. Leveraging elastic instabilities for amplified performance: Spine-inspired high-speed and high-force soft robots. *Sci. Adv.* **2020**, *6*, eaaz6912. [CrossRef]
65. Gorissen, B.; Melancon, D.; Vasios, N.; Torbati, M.; Bertoldi, K. Inflatable soft jumper inspired by shell snapping. *Sci. Robot.* **2020**, *5*, eabb1967. [CrossRef]
66. Fu, H.; Nan, K.; Bai, W.; Huang, W.; Bai, K.; Lu, L.; Zhou, C.; Liu, Y.; Liu, F.; Wang, J. Morphable 3D mesostructures and microelectronic devices by multistable buckling mechanics. *Nat. Mater.* **2018**, *17*, 268–276. [CrossRef] [PubMed]
67. Li, J.; Tanaka, H. Rapid customization system for 3D-printed splint using programmable modeling technique—A practical approach. *3D Print. Med.* **2018**, *4*, 5. [CrossRef]
68. Guerra, A.J.; Cano, P.; Rabionet, M.; Puig, T.; Ciurana, J. 3D-Printed PCL/PLA Composite Stents: Towards a New Solution to Cardiovascular Problems. *Materials* **2018**, *11*, 1679. [CrossRef]
69. Larush, L.; Kaner, I.; Fluksman, A.; Tamsut, A.; Pawar, A.A.; Lesnovski, P.; Benny, O.; Magdassi, S. 3D printing of responsive hydrogels for drug-delivery systems. *J. 3D Print. Med.* **2017**, *1*, 219–229. [CrossRef]
70. Randall, C.L.; Gultepe, E.; Gracias, D.H. Self-folding devices and materials for biomedical applications. *Trends Biotechnol.* **2012**, *30*, 138–146. [CrossRef]
71. Milazzo, M.; Negrini, N.C.; Scialla, S.; Marelli, B.; Farè, S.; Danti, S.; Buehler, M.J. Additive Manufacturing Approaches for Hydroxyapatite-Reinforced Composites. *Adv. Funct. Mater.* **2019**, *29*, 1903055. [CrossRef]
72. Gao, B.; Yang, Q.; Zhao, X.; Jin, G.; Ma, Y.; Xu, F. 4D bioprinting for biomedical applications. *Trends Biotechnol.* **2016**, *34*, 746–756. [CrossRef] [PubMed]
73. Guo, R.; Li, Z.; Jiang, Z.; Yuan, D.; Huang, W.; Xia, A. Log-pile photonic crystal fabricated by two-photon photopolymerization. *J. Opt. A Pure Appl. Opt.* **2005**, *7*, 396–399. [CrossRef]
74. Farsari, M.; Chichkov, B.N. Two-photon fabrication. *Nat. Photonics* **2009**, *3*, 450–452. [CrossRef]
75. Ergin, T.; Stenger, N.; Brenner, P.; Pendry, J.B.; Wegener, M. Three-dimensional invisibility cloak at optical wavelengths. *Science* **2010**, *328*, 337–339. [CrossRef]
76. Hahn, V.; Mayer, F.; Thiel, M.; Wegener, M. 3-D laser nanoprinting. *Opt. Photonics News* **2019**, *30*, 28–35. [CrossRef]
77. Nocentini, S.; Riboli, F.; Burresi, M.; Martella, D.; Parmeggiani, C.; Wiersma, D.S. Three-dimensional photonic circuits in rigid and soft polymers tunable by light. *ACS Photonics* **2018**, *5*, 3222–3230. [CrossRef]
78. Scarpa, E.; Lemma, E.D.; Fiammengo, R.; Cipolla, M.P.; Pisanello, F.; Rizzi, F.; De Vittorio, M. Microfabrication of pH-responsive 3D hydrogel structures via two-photon polymerization of high-molecular-weight poly (ethylene glycol) diacrylates. *Sens. Actuators B Chem.* **2019**, *279*, 418–426. [CrossRef]
79. Tudor, A.; Delaney, C.; Zhang, H.; Thompson, A.J.; Curto, V.F.; Yang, G.-Z.; Higgins, M.J.; Diamond, D.; Florea, L. Fabrication of soft, stimulus-responsive structures with sub-micron resolution via two-photon polymerization of poly ionic liquids. *Mater. Today* **2018**, *21*, 807–816. [CrossRef]
80. Lu, D.-X.; Zhang, Y.-L.; Han, D.-D.; Wang, H.; Xia, H.; Chen, Q.-D.; Ding, H.; Sun, H.-B. Solvent-tunable PDMS microlens fabricated by femtosecond laser direct writing. *J. Mater. Chem. C* **2015**, *3*, 1751–1756. [CrossRef]